Elastic scattering and transfer reactions for the system ^{7}Be + ^{58}Ni at Coulomb barrier energies

2015 J. Phys.: Conf. Ser. 639 012002

(http://iopscience.iop.org/1742-6596/639/1/012002)

Elastic scattering and transfer reactions for the system ^{7}Be + ^{58}Ni at Coulomb barrier energies

M. Mazzocco[1,2], D. Torresi[1,2], L. Acosta[3], A. Boiano[4], C. Boiano[5], T. Glodariu[6], A. Guglielmetti[7,5], N. Keeley[8], M. La Commara[9,4], J.A. Lay[1,2], I. Martel[3], C. Mazzocchi[7,5], P. Molini[1,2], C. Parascandolo[4], V.V. Parkar[3], D. Pierroutsakou[4], M. Romoli[4], K. Rusek[10], A.M. Sanchez-Benitez[3], M. Sandoli[9,4], C. Signorini[1,2], R. Silvestri[9,4], F. Soramel[1,2], E. Strano[1,2], L. Stroe[6]

[1] Dipartimento di Fisica e Astronomia, Università di Padova, via F. Marzolo 8, I-35131 Padova, Italy
[2] INFN-Sezione di Padova, via F. Marzolo 8, I-35131 Padova, Italy
[3] Departamento de Fìsica Aplicada, Universidad de Huelva, Campus de El Carmen, E-21071 Huelva, Spain
[4] INFN-Sezione di Napoli, via Cintia, I-80126, Napoli, Italy
[5] INFN-Sezione di Milano, via Celoria 16, I-20133, Napoli, Italy
[6] NIPNE, 407 Atomistilor Street, 077125 Magurele, Romania
[7] Dipartimento di Fisica, Università di Milano, via Celoria 16, I-20133 Padova, Italy
[8] Department of Nuclear Reactions, Institute for Nuclear Studies, ul. Hoza 69, 00-681 Warsaw, Poland
[9] Dipartimento di Fisica, Università di Napoli "Federico II", via Cintia, I-80126, Napoli, Italy
[10] Heavy Ion Laboratory, University of Warsaw, ul. Pasteura 5a, 02-093 Warsaw, Poland

E-mail: marco.mazzocco@pd.infn.it

Abstract. We investigated the reaction induced by the Radioactive Ion Beam ^{7}Be on the closed proton shell nucleus ^{58}Ni at 22.0 MeV bombarding energy. The ^{7}Be beam was produced by means of the in-flight technique with the facility EXOTIC at INFN-LNL (Italy). Charged reaction products were mass and charge identified in a rather wide angular range and their energy distributions were analyzed to infer some information on the production mechanism. The relevance of direct processes, especially ^{3}He- and ^{4}He-stripping, as well as compound nucleus reactions is critically reviewed.

1. Introduction

Light atomic nuclei, even very close to the valley of β-stability, may exhibit very exotic features. The reduced number of nucleons and the incredibly high binding energy of the ^{4}He nucleus can give rise to very peculiar nuclear shapes. For instance, ^{6}He is a well-known 2n-halo nucleus, that can be easily described as a ^{4}He core surrounded by two weakly-bound neutrons (S_{2n} = 0.972 MeV). Other typical examples of halo nuclei are the 2n-halo ^{11}Li (S_{2n} = 0.300 MeV), the 1n-halo ^{11}Be (S_n = 0.504 MeV) and the 1p-halo ^{8}B (S_p = 0.1375 MeV).

When a halo projectile approaches a target nucleus, the rarefied nuclear matter surrounding the well-bound core should intuitively lower the Coulomb barrier, thus enhancing the fusion probability. In heavy-ion collisions it is rather well established that the nuclear deformation

increases the fusion cross cross by several orders of magnitude [1]. However, differently from heavy ions, halo nuclei are generally very weakly-bound and the projectiles can more easily break in the nuclear and Coulomb field provided by the target nucleus. In such a circumstance, the breakup process would reduce the incoming flux and, consequently, the fusion probability. The question whether halo structure and low breakup threshold would enhance or hinder the fusion cross sections has puzzled the nuclear physics community for twenty years at least. Several review papers have been written on this topic (see, for example, [2]).

Unfortunately, all halo nuclei are unstable and the intensities of presently available Radioactive Ion Beams (RIBs) are still, in the best cases, few orders of magnitude lower than stable beams. Therefore, studies involving halo nuclei are very challenging and may suffer of low statistical accuracy. Recent experiments helped achieving a (tentative) systematic description of breakup related effects on the reaction dynamics at Coulomb barrier energies. It is in fact quite well established that the halo properties enhance the reaction probability rather than the fusion cross section. The question has now moved towards understanding what reaction mechanisms are mainly responsible for the total reaction probability enhancement. Experiments performed with the 2n-halo ^{6}He [3, 4, 5, 6] and the neutron skin nucleus ^{8}He [7, 8] indicated transfer channels, especially 1n- and 2n-stripping, as the main candidates. On the other side, data collected with the 1p-halo ^{8}B [9] and the 2n-halo ^{11}Li [10, 11] suggested that the major contribution was coming from the breakup channel. Finally the statistics collected for the 1n-halo ^{11}Be [12] did not allow to determine whether the large yield of ^{10}Be observed was mostly due to the 1n-stripping or to the breakup process.

Within this framework, we undertook the study of the weakly-bound nucleus ^{7}Be, a radioactive nucleus with a low particle emission threshold (S_α = 1.586 MeV) and a well pronounced ^{3}He-^{4}He cluster structure in the ground state. The main feature of ^{7}Be-induced reactions is that all the most relevant reaction channels (breakup process, transfer channels) produce only stable well-bound particles in the exit channel, without requiring the low-efficiency detection of neutrons, as in all studies of n-halo nuclei, or the detection of weakly-bound or radioactive fragments, which can easily break up or decay thus further complicating the reconstruction of the reaction dynamics scenario at Coulomb barrier energies. As first experiment, we studied the interaction of the ^{7}Be RIB with the closed proton shell nucleus ^{58}Ni at 22.0 MeV bombarding energy.

The contribution is organized as follows: Sect. 2 will describe the facility EXOTIC and the technique employed for the production of the ^{7}Be RIB. Sect. 3 will present the experimental set-up used for studying the reaction ^{7}Be + ^{58}Ni. The data analysis for the elastic scattering process and for the ^{3,4}He production will be covered in Sects. 4 and 5, respectively. Some concluding remarks will be drawn in Sect. 6.

2. The facility EXOTIC

In 2001 we started to lay out a small facility [13] for the in-flight production of light weakly-bound RIBs. The facility is located at the Laboratori Nazionali di Legnaro (LNL, Italy) of the Istituto Nazionale di Fisica Nucleare (INFN). RIBs are produced via two-body inverse kinematics reactions induced by heavy-ion beams, delivered by the LNL-XTU Tandem accelerator, impinging on light gas target. The target station consists of a 5-cm long gas cell doubly-walled with 2.2-μm thick havar windows. The gas cell is routinely filled with H_2, D_2 and ^{3}He gases up to an internal pressure of 1.2 bar and can be operated either at room (300 K) or cryogenic (90 K) temperature.

The facility EXOTIC is made up by eight ion-optical elements: a first quadrupole triplet, a 30° dipole bending magnet, a 1-m long Wien filter and a second quadrupole triplet. The combined selection in magnetic rigidity and velocity, provided by the dipole magnet and by the Wien filter, respectively, helped achieving secondary beam purities as good as 98-99% for the

^{7}Be, ^{8}Li, ^{15}O and ^{17}F secondary beams. A complete list of RIBs which can be produced with the facility EXOTIC can be found in Ref. [14].

Over the last 10 years, several experiments aimed at investigating the reaction dynamics induced by light weakly-bound RIBs at Coulomb barrier energies were performed with the facility EXOTIC. We studied the elastic scattering process for the systems ^{17}F + ^{1}H [15], ^{17}F + ^{58}Ni [16], ^{17}F + ^{208}Pb [17], ^{8}Li + ^{90}Zr [18] and the fusion process for the reaction ^{8}B + ^{28}Si [19]. More recently, the capabilities of the facility to be used as a separator for heavy-ion fusion evaporation residues were also successfully tested.

3. Experiment

The RIB ^{7}Be for the present experiment was produced by means of the two-body reaction $p(^{7}\mathrm{Li},^{7}\mathrm{Be})n$ (Q_{value} = -1.97 MeV). A 34.2 MeV ^{7}Li primary beam with an intensity of 70-100 pnA was impinging on the target cell filled with $^{1}H_2$ gas at a pressure of about 1 bar and kept at liquid nitrogen temperature. The resulting ^{7}Be beam had an energy of 22.0 $\pm$ 0.4 MeV, an average intensity of 2 $\times$ 10^5 pps and a 99%-purity.

Charged reaction products originated from the interaction of the RIB with a 1 mg/cm^2 ^{58}Ni target were detected by means of 3 two-stage ΔE-E$_{res}$ telescopes [20]. The ΔE and E$_{res}$ stages were 40-42 μm and 1 mm thick, respectively, Double Sided Silicon Strip Detectors (DSSSDs). All DSSSDs had an active area of 48.5 mm $\times$ 48.5 mm and were segmented into 16 strips per side, thus defining a 3 mm $\times$ 3 mm pixel structure. Two telescopes were located at forward angles, T1 (T2) in the left (right) hemisphere at a mean polar angle θ_{lab} = +57.1° (-63.5°) and at a distance of 73 (70) mm from the target. The third telescope (T3) was displaced at a mean polar angle θ_{lab} = -134.2° and at a distance of 71.5 mm from the target.

4. Elastic scattering

The first step of the data analysis consisted in the evaluation of the differential cross section for the elastic scattering process. We performed the reaction Q_{value} reconstruction for all events releasing more than 10 MeV in the telescope ΔE stages. The ^{7}Be scattering energy, in fact, was not sufficient to punch through the inner stage of the telescopes to allow the unambiguous identification by means of the ΔE-E$_{res}$ technique. A threshold value of 10 MeV in the ΔE energy loss was chosen to avoid, especially at backward angles, the selection of Z=2 reaction products and to minimize possible contributions from Z=3 nuclei.

The reaction Q_{value} is defined as the difference between the kinetic energy of the reaction entrance and exit channel, as described in the following formula:

$$Q_{value} = E_{scattering} + E_{recoil} - E_{beam} \tag{1}$$

where $E_{scattering}$, E_{recoil} and E_{beam} are the ^{7}Be scattering energy, the ^{58}Ni recoil energy and ^{7}Be incoming energy, respectively. The (undetected) target recoil energy was reconstructed via linear momentum conservation. Being $\vec{p}_{initial}$ and $\vec{p}_{final}$ the overall linear momenta of the initial and final state, respectively, we can write the following equations:

$$\vec{p}_{initial} = \vec{p}_{final} \tag{2}$$

$$\vec{p}_{beam} + \vec{p}_{target} = \vec{p}_{scattering} + \vec{p}_{recoil} \tag{3}$$

$$\vec{p}_{beam} = \vec{p}_{scattering} + \vec{p}_{recoil} \tag{4}$$

where $\vec{p}_{beam}$, $\vec{p}_{target}$(=0), $\vec{p}_{scattering}$ and $\vec{p}_{recoil}$ are the beam, target (at rest), scattered particle and recoil nucleus momenta, respectively. We can therefore derive the following expression for the momentum of ^{58}Ni recoiling nuclei:

$$\vec{p}_{recoil} = \vec{p}_{beam} - \vec{p}_{scattering} \tag{5}$$

then, considering the individual components, we obtain:

$$\vec{p}_{recoil,x} = -\sqrt{2M_{scattering}E_{scattering}}\sin\theta\cos\phi \tag{6}$$

$$\vec{p}_{recoil,y} = -\sqrt{2M_{scattering}E_{scattering}}\sin\theta\sin\phi \tag{7}$$

$$\vec{p}_{recoil,z} = \sqrt{2M_{beam}E_{beam}} - \sqrt{2M_{scattering}E_{scattering}}\cos\theta \tag{8}$$

where $M_{beam} = M_{scattering}$ is the projectile mass. The polar angle θ and the azimuthal angle ϕ are calculated (in the laboratory frame) by randomizing the position of the scattered particle within the fired detector pixel and assuming that the particle trajectory originated from the target center. Black circles in Figs. 1 and 2 represent the result of this procedure for the experimental data collected at forward and backward angles by telescope T1 and T3, respectively. Events are essentially distributed around $Q_{value} = 0$, as expected for a pure elastic scattering process.

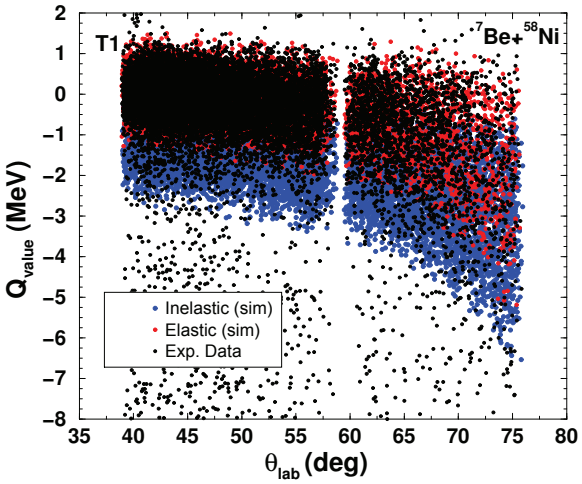

Figure 1. Q_{value} *vs.* detection angle θ_{lab} correlation plot for telescope T1 located at forward angles. Black circles represent the experimental data, while red and blue dots are the results of Monte-Carlo simulations for the elastic scattering process and for inelastic excitations leading to the target first excited state, respectively. See text for additional details.

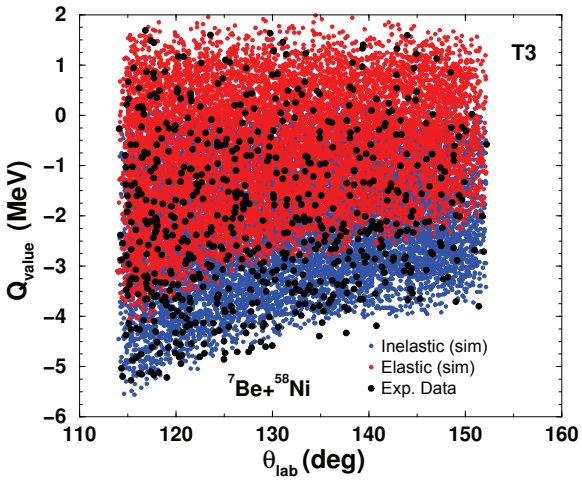

Figure 2. Same as Fig. 1, but for the telescope T3 located at backward angles.

This analysis technique accounts for most of the effects related to the reaction kinematics, however the use of a relatively low-energy beam ($\sim$ 3 MeV/u) and of a quite thick target (1 mg/cm^2) introduces a distortion in the Q_{value} reconstruction procedure in the region around θ_{lab} = 90°. To test the effects of the target thickness, we performed a Monte-Carlo simulation of the elastic scattering process taking into account the secondary beam energy spread, the beam spot on target, the energy loss into the target before and after the scattering process, the displacement of the telescopes around the target and the detector experimental energy resolution. The results are displayed with red dots in Figs. 1 and 2. We then carried out a similar simulation also for inelastic excitations leading to the projectile and target first excited states at 0.429 MeV

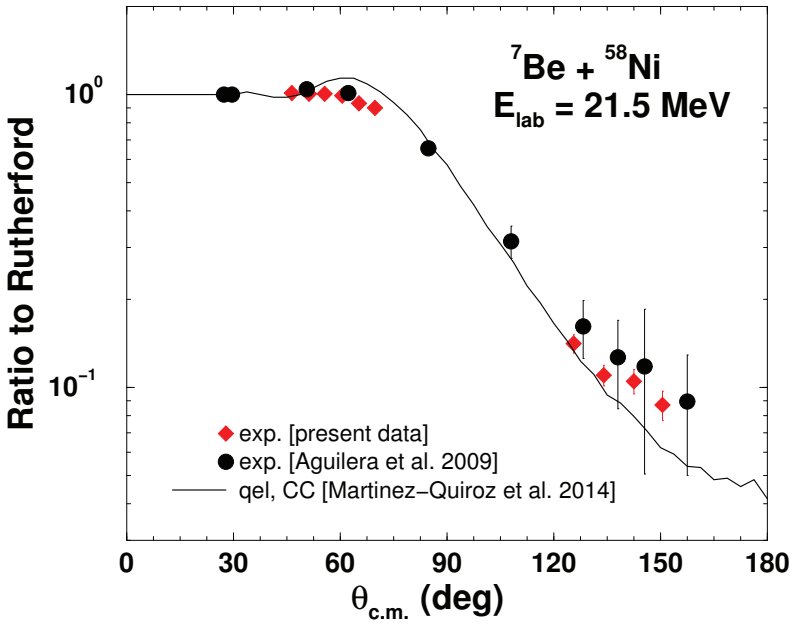

Figure 3. Differential cross section for the "quasi-elastic" process in the reaction ^{7}Be + ^{58}Ni at 21.5 MeV. Red diamonds correspond to the present measurement, while black circles originate from an earlier experiment performed by E.F. Aguilera and collaborators. The continuous line represents the theoretical prediction recently published in [21]

and 1.454 MeV, respectively, and represented the results for the latter process with blue dots in the same figures. At forward angles, the experimental data are clearly compatible with the kinematics of a pure elastic scattering. The scenario is slightly more complicated at backward angles, where we cannot recognize a net distinction in the distribution of the experimental data between the region where we expected to detect elastic events and that where we should observe only inelastic processes. Therefore in the data analysis we selected experimental events detected in both regions and the resulting angular distribution, depicted with red diamonds in Fig. 3, has to be considered the differential cross section for the "quasi-elastic" process.

Fig. 3 also shows that our evaluation remarkably agrees with the earlier measurement [9] at about the same beam energy by E.F. Aguilera and coworkers and with the theoretical predictions more recently published by the same group [21]. To account for the energy loss into the target ($\sim$ 1 MeV) we indicated in Fig. 3 the beam energy at the mid-target position (21.5 MeV).

5. ^{3,4}He production

Fairly large production yields for both ^{7}Be constituent clusters, ^{3}He and ^{4}He, were observed both at forward and backward angles. As a matter of fact, ^{4}He ions resulted to be 4-5 times more abundant than ^{3}He. This outcome, together with the fact that we did not observe any ^{3}He-^{4}He coincidences, already rules out the possibility that both ^{3}He and ^{4}He are uniquely produced by the breakup process ^{7}Be $\rightarrow$ ^{3}He + ^{4}He. In such a circumstance, comparable yields for both helium isotopes should have been recorded.

Several processes can contribute to the production of ^{3}He and ^{4}He. In the present contribution we discuss the cases of the ^{3}He-stripping, ^{4}He-stripping and complete fusion. Other reaction mechanisms, such as n-pick and n-stripping, will be covered in a more extended publication.

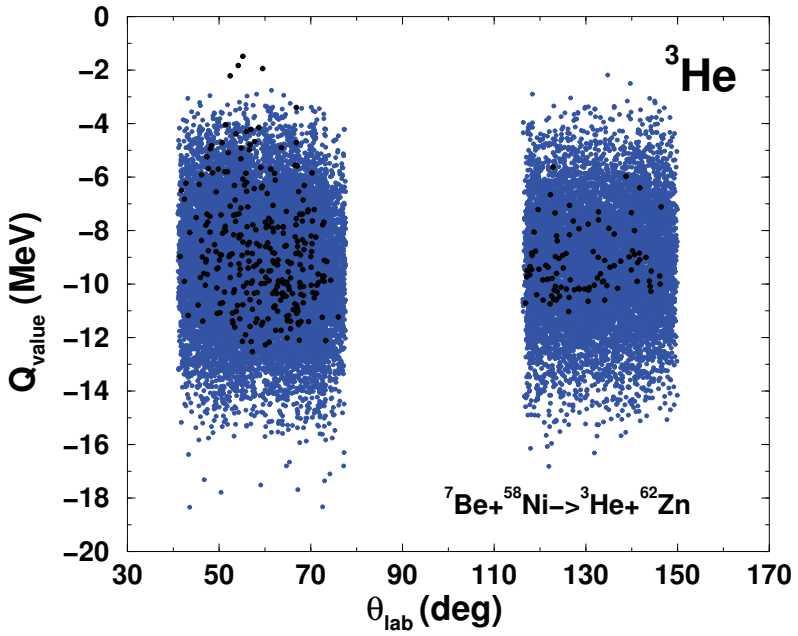

Figure 4. Q_{value} *vs.* θ_{lab} correlation plot for ^{3}He ions. Black circles represent the experimental data, while blue dots are the results of a Monte-Carlo simulation for the ^{4}He-stripping process. Additional details can be found in the text.

5.1. ^{3}He production

We performed the Q_{value} reconstruction assuming that all ^{3}He particles originated from the ^{4}He-stripping process: ^{7}Be + ^{58}Ni → ^{3}He + ^{62}Zn (ground-state-to-ground-state Q_{value} (Q_{gg}) = +1.78 MeV). In this case, $M_{scattering}$, $E_{scattering}$ and $\vec{p}_{scattering}$ in Eqs. 1-8 represent the ^{3}He mass, energy and linear momentum, respectively. The results of the procedure are displayed with black circles in Fig. 4. The semi-classical model of Brink [22] foresees an optimum Q_{value} (Q_{opt}) for the ^{4}He-stripping process of about -8.96 MeV and the experimental data in Fig. 4 are rather symmetrically distributed around -9 MeV.

We also performed a Monte-Carlo simulation for the ^{4}He-stripping process and we depicted the results with blue dots in Fig. 4. In the code, we assumed that the transfer process was proceeding to a final state distribution of the target-like particle with a mean excitation energy E_x (= Q_{gg} - Q_{opt}) = 10.7 MeV and a standard deviation of 2.0 MeV. The good agreement between experimental and simulated data, clearly evident in Fig. 4, reinforces the initial assumption that ^{3}He ions were mostly generated by the ^{4}He-stripping reaction mechanism.

5.2. ^{4}He production

The Q_{value} reconstruction procedure was undertaken also for ^{4}He ions, to verify whether their energy distribution could be compatible with a ^{3}He-stripping (^{7}Be + ^{58}Ni → ^{4}He + ^{61}Zn, Q_{gg} = +9.46 MeV) as main triggering mechanism. Also in this case the semi-classical model of Brink predicts an Q_{opt} of about -8.96 MeV. Fig. 5 shows that experimental data are essentially distributed around Q_{value} = -9 MeV, but also extend with continuity up to $Q_{value} \approx 0$ MeV. Moreover, the minimum energy required for ^{4}He ions to pass through the ΔE thickness (7.3 MeV) introduces a threshold in the Q_{value} reconstruction procedure. Such a threshold increases as the detection polar angle gets larger and explains the reason why we almost did not observe events with Q_{value} smaller than -10 MeV at backward angles. This effect is particularly visible

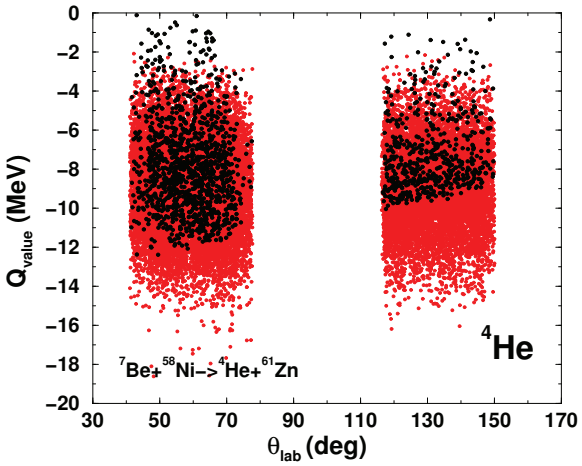

Figure 5. Same as Fig. 4, but for ^{4}He ions and for the ^{3}He-stripping process.

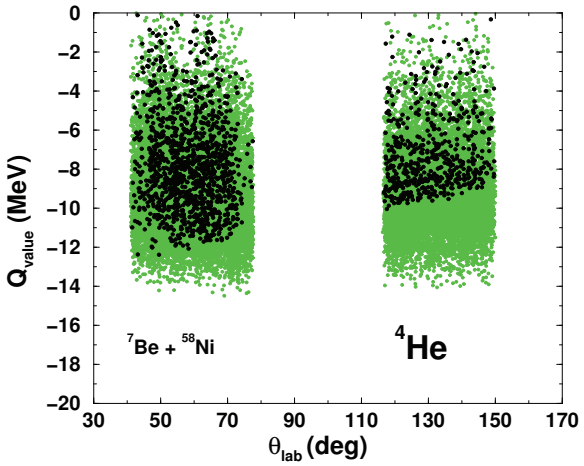

Figure 6. Same as Fig. 5, but for complete fusion process.

when we compare the results of the Monte-Carlo simulation for the ^{3}He-stripping process (red dots in Fig. 5) with the experimental data. In addition, Fig. 5 shows that the ^{3}He-stripping process cannot account for events with reconstructed Q_{value} larger than $\sim$ -3 MeV.

We therefore employed the code PACE2 [23], based on the statistical model, to compute the energy and angular distribution of α particles emitted after a compound nucleus reaction. From an experimental point of view, we do not know a priori the reaction mechanism which produces ^{4}He ions. However, if we apply the the Q_{value} reconstruction procedure to fusion-evaporation events assuming that they were generated from the ^{3}He-stripping process, we can somehow mimic the experimental conditions. The results, displayed in Fig. 6 with green dots, illustrate that both processes foresee very similar energy/Q_{value} distributions. Nevertheless, high energetic ^{4}He ions can more easily originate from a complete fusion process, especially at backward angles, rather than from the ^{3}He-stripping process, but in any case we cannot single out the individual components of the two processes taking into account only the ^{4}He energy distribution.

5.3. ^{3,4}He angular distributions

Fig. 7 show the preliminary evaluation of the angular distribution for the two helium isotopes. The angle-integrated cross section for the ^{3}He production is 34.4 $\pm$ 6.3 mb. For ^{4}He, we can tentatively estimate the contribution arising from the fusion process, by computing the angular distribution for evaporated α particles with the code PACE2 and using the ^{4}He data collected at backward angles for the normalization. This approach gives a cross section of 161.5 $\pm$ 11.5 mb for the ^{4}He evaporation channel. If we subtract this contribution from the total ^{4}He production yield, we obtain an overall cross section of 44.1 $\pm$ 9.9 mb for direct processes.

6. Summary

We measured for the first time the energy and angular distribution of ^{3}He and ^{4}He ions produced in the nuclear collision between a ^{7}Be RIB and a ^{58}Ni target at 22.0 MeV beam energy. The experimental data were analyzed by means of the Q_{value} reconstruction procedure. Several different processes can contribute to the production of these two helium isotopes. According to our analysis, ^{3}He ions originate essentially from the ^{4}He-stripping process. On the other side, ^{4}He nuclei are mostly generated after a fusion-evaporation process, with substantial contributions from direct processes, in primis, the ^{3}He-stripping channel. Additional work is currently in

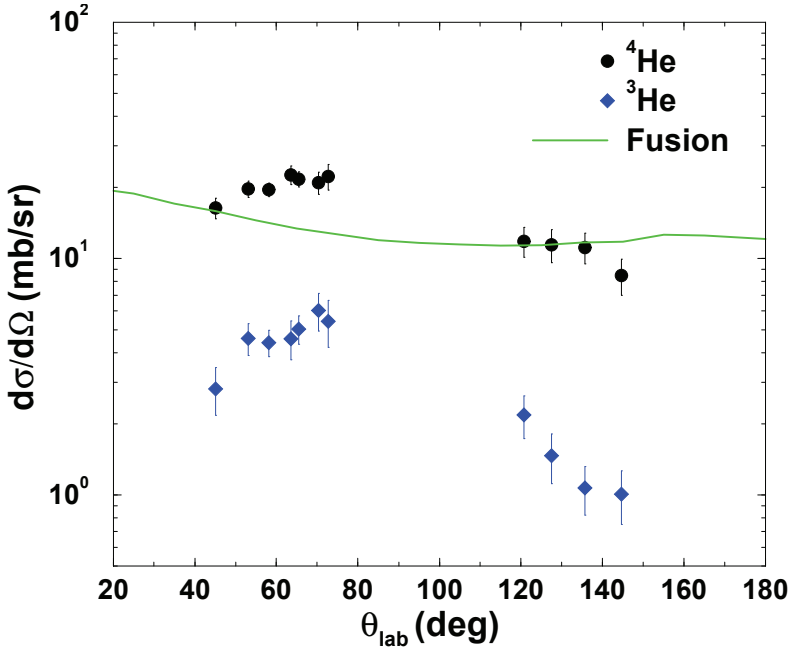

Figure 7. ^{3}He (blue diamonds) and ^{4}He (black circles) angular distributions. The green continuous line represents the angular distribution predicted by the statistical code PACE2 for α particles evaporated after a compound nucleus reaction.

progress to estimate possible contributions arising from the n-pick and the n-stripping transfer processes and from the breakup channel.

References

[1] Dasgupta M et al. 1998 *Ann. Rev. Nucl. Part. Sci.* **48** 401
[2] Canto L F et al. 2006 *Phys. Rep.* **424** 1
[3] Raabe R et al. 2004 *Nature* **431** 823
[4] Di Pietro A et al. 2004 *Phys. Rev. C* **69** 044613
[5] Navin A et al. 2004 *Phys. Rev. C* **69** 044601
[6] Kolata J J et al. 2007 *Phys. Rev. C* **75** 031302(R)
[7] Lemasson A et al. 2009 *Phys. Rev. Lett.* **103** 232701
[8] Lemasson A et al. 2010 *Phys. Rev. C* **82** 044617
[9] Aguilera E F et al. 2009 *Phys. Rev. C* **79** 021601(R)
[10] Cubero M et al. 2012 *Phys. Rev. Lett.* **109** 262701
[11] Fernandez-Garcia J P et al. 2013 *Phys. Rev. Lett.* **110** 142701
[12] Di Pietro A et al. 2010 *Phys. Rev. Lett.* **105** 022701
[13] Farinon F et al. 2008 *Nucl. Instrum. Meth. B* **266** 4097
[14] Mazzocco M et al. 2013 *Nucl. Instrum. Meth. B* **317** 223
[15] Patronis N et al. 2012 *Phys. Rev. C* **85** 024609
[16] Mazzocco M et al. 2010 *Phys. Rev. C* **82** 054604
[17] Signorini C et al. 2010 *Eur. Phys. J. A* **44** 63
[18] Pakou A et al. 2015 *Eur. Phys. J. A* (in press)
[19] Pakou A et al. 2013 *Phys. Rev. C* **87** 014619
[20] Sanchez-Benitez A M et al. 2005 *J. Phys. G* **31** S1953
[21] Martinez-Quiroz E et al. 2014 *Phys. Rev. C* **90** 014616
[22] Brink D M 1972 *Pyhs. Lett. B* **40** 37
[23] Gavron A 1980 *Phys. Rev. C* **21** 230